ACS OMEGA

http://pubs.acs.org/journal/acsodf

Article

Characterization and *In Vitro* Evaluations of Injectable Calcium Phosphate Cement Doped with Magnesium and Strontium

Vetharaj HephzibahRajam Arkin, Uttamchand Narendrakumar, Harishkumar Madhyastha, and Inderchand Manjubala*

Cite This: *ACS Omega* 2021, 6, 2477−2486

Read Online

ACCESS | Metrics & More | Article Recommendations

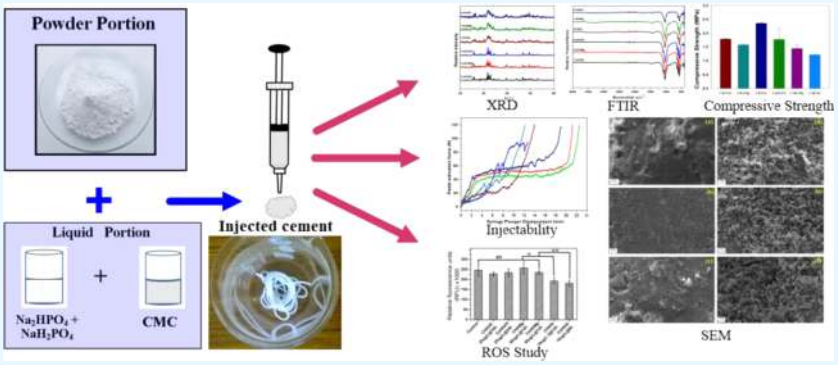

ABSTRACT: Injectable calcium phosphate cement is a promising biomaterial for hard tissue repair due to its osteoinductivity, biocompatibility properties, and its use to correct defect areas involving narrow cavities with limited accessibility by the minimally invasive technique. Microwave-synthesized hydroxyapatite (HA) was used for the preparation of cement. In recent years, both magnesium and strontium calcium phosphate cements have exhibited rapid setting, improved mechanical strength, and a good resorption rate. A big step still remains to develop injectable magnesium and strontium phosphate cements with ideal self-setting properties, adequate mechanical strength, and good biocompatibility for clinical applications. In this study, both magnesium and strontium were doped with synthesized semiamorphous and crystalline hydroxyapatite (HA). The powder mixture was mixed with Na_2HPO_4, NaH_2PO_4, and a carboxymethyl cellulose (CMC) solution to develop the novel magnesium and strontium calcium phosphate cement. The setting time, physiochemical properties of hardened cement, microstructure, mechanical strength, and injectability of the prepared cement were studied. The toxicity evaluation and cell adhesion, which are necessary to identify the suitability of the material for different applications, were quantified and investigated using fibroblast cells. The setting time of cement was reduced substantially for magnesium- or strontium-doped cement by 2 min. The phase composition of the hardened cement expresses the semiamorphous or crystalline phase of HA with additives. Smooth and complete injection of cement paste was observed in semiamorphous HA-based cement. The intercellular reactive oxygen stress (ROS) of the Sr^{2+}-doped cement sample showed varied degrees of toxicity to cells in terms of different concentrations. The Mg^{2+}-doped cement showed significant attachment of cells after treatment at varying incubation times.

1. INTRODUCTION

Every year, about 2.2 million people worldwide need replacement surgeries and bone grafting for repairing critical-size large bony defects that come to light from accidents and trauma-related causes.[1] Different types of calcium phosphate (CaP)-based biomaterials as bone substitute materials are widely recognized in clinical applications due to their excellent biocompatibility and osteoconductivity.[2] Hydroxyapatite (HA) is one of the most commonly used CaP in bone tissue engineering. The inorganic constituents of bones and teeth are similar to those of synthetic HA in terms of properties and chemical formulae. Thus, artificial bone grafts composed of synthetic HA have been widely used as biomaterials for repairing and substituting hard tissues due to their exceptional bioactive, biocompatible, osteoconductive, and osteointegrative effects.[3,4]

The physiological characteristics of bones are their self-healing and remodeling capacity. These characteristics become

Received: August 14, 2020
Accepted: January 4, 2021
Published: January 20, 2021

https://dx.doi.org/10.1021/acsomega.0c03927
ACS Omega 2021, 6, 2477−2486

inadequate in cases of critical-size defects that are observed in orthopedic, maxillofacial, and dental surgeries, which may lead to extensive bony defects.[5] Calcium phosphate-based cements (CPCs) are the most frequently researched category of bone cement. Calcium phosphate cement is prepared by mixing reactive calcium phosphate powders with an aqueous solution.[6,7] CPCs are divided into two main forms based on the different pH-dependent solubilities of cement reactants and the final product, namely, hydroxyapatite (HA) or dicalcium phosphate dihydrate (DCP, brushite). Ideally, CPCs should possess parameters like favorable setting time, injectability, optimal mechanical properties, support of cell adhesion, proliferation, and stimulation of osteogenesis.[8]

In recent years, the evolution of injectable CPCs has gained much attention. These injectable CPCs used for augmentation of osseous defects have potential clinical applications in oral implants, as well as fixation of orthopedic implants and grafts.[9,10] Injectable cement paste is used to correct defect areas involving narrow cavities with limited accessibility by the minimally invasive technique.[11] The aqueous-based self-setting injectable inorganic cement generally undergoes phase separation during injection through a syringe and needle in clinical applications, which is a major limitation.[12] The viscosity of the liquid phase enhances the injectability of CPC by including the aqueous solution containing methylcellulose and hydroxypropyl methylcellulose.[13,14] In this study, we use carboxymethyl cellulose (CMC), a nontoxic, hydrophilic polymer,[15] that makes an excellent candidate for improvement of injectability without phase separation and it can bond with calcium phosphate particles.[16]

The ideal choice to enhance the bioactive properties of CPC is by doping ions in the cement paste. Magnesium ions (Mg^{2+}) are naturally found in bones and play a key role in bone metabolism, as they are the fourth most abundant cations in the human body.[17,18] It has been lately proposed that magnesium calcium phosphate cement (MCPC) indirectly influences the mineral metabolism and acts as an essential factor in the qualitative changes in the bone matrix.[19,20] Mg^{2+} ions in CPC can decrease the setting time and is reported as a potential biocompatibility bone material. Besides the setting time and biocompatibility, in comprehensive *in vitro* studies, it is found that the release of Mg^{2+} ions in CPC enhances the activity of osteoblast differentiation[21] and inhibits osteoclast formation,[22] which is an important aspect that should be taken into account for a biomaterial. Meanwhile, in various research studies over the last few years, strontium(II) (Sr^{2+}) has been proven effective in the stimulation of osteogenesis and acts as a bone resorption inhibitor.[23] The addition of strontium into standard poly(methyl methacrylate) (PMMA)-based cement can be used for the treatment of osteoporotic bone fractures. Sr^{2+} ions can be replaced with Ca^{2+} due to chemical similarity, giving rise to impairing the possibility to participate in a cement reaction to a variety of possible strontium-containing calcium phosphate cements. Guo et al. were the first to add Sr^{2+} ions into CPC by replacing strontium hydrogen phosphate ($SrHPO_4$) with calcium hydrogen phosphate ($CaHPO_4$) in a tetracalcium phosphate cement.[24] *In vitro* and *in vivo* studies revealed that Sr^{2+} ions acts both as an inhibitor of resoprtion and as a stimulus of bone formation.[23] Also, recent studies have shown that higher dose administration of strontium ranelate has rarely been connected to osteomalacia in rats.[25,26]

In this study, magnesium and strontium were added independently to both semiamorphous and crystalline HA and were used as precursors in cement preparation to know the effects of crystallinity on the injectable force as well as study the effects of Mg^{2+} and Sr^{2+} ions on the setting time, mechanical strength, and *in vitro* toxicity with respect to concentration and time of exposure.

2. MATERIALS AND METHODS

2.1. Materials. The materials used in this study were dicalcium phosphate anhydrous (DCPA, $CaHPO_4$), calcium carbonate ($CaCO_3$), magnesium carbonate ($MgCO_3$), strontium carbonate ($SrCO_3$), monosodium hydrogen phosphate (NaH_2PO_4), disodium hydrogen phosphate (Na_2HPO_4), and carboxymethyl cellulose (CMC) sodium salt; they were purchased from HiMedia, India, and were used without further purification. Minimum essential medium (MEM) and crystal violet cell stain medium were procured from Sigma-Aldrich Co., Ltd. (Sigma-Aldrich, St. Louis, MO).

2.2. Preparation of Calcium Phosphate Cement. The HA powder was prepared using the procedure of Manjubala et al.[27] and was used as a starting material. In brief, HA was prepared using a domestic microwave oven (LG India, 2.45 GHz, 800 W) and was named CHA. A part of the CHA powder was sintered at 900 °C for 12 h to increase crystallinity and was named SHA. The calcium phosphate cement was prepared with a solid/liquid-phase reaction, where the liquid/powder ratio was 0.45 mL/g, using the standard procedure of Takagi and Chow.[28] The solid phase consisted of 76 wt % HA (or SHA), 20 wt % DCPA, and 4 wt % $CaCO_3$. Invariants of CPC and $CaCO_3$ were reduced to 2 wt %, and 2 wt % of $MgCO_3$ or $SrCO_3$ was added. The liquid phase was prepared using equivolume of 0.25 M Na_2HPO_4, NaH_2PO_4, and a 2.5 wt % of the CMC solution. All of the powders were homogeneously mixed and the cement paste was prepared in a glass plate by dropwise addition of the liquid mixture. The prepared paste was then filled in a die mold (6 mm diameter × 3 mm height) and was used for setting time measurements. The paste was then filled immediately in a syringe for injectability measurements.

2.3. Setting Time Evaluation. The setting time, initial and final time (I_t and F_t) of the cement, was determined at room temperature using Gillmore needles. The prepared paste was pressed using a mixing spatula into a cylindrical disc-shaped stainless steel mold die (6 mm diameter × 3 mm height) and was allowed to set at room temperature. The setting time of each cement sample was checked using the initial setting time of the needle tip (diameter = 2.12 mm and weight = 113.4 g) and the final setting time of the needle tip (diameter = 1.06 mm and weight = 453.6 g). The time of setting was determined by holding the needle in a vertical position and lightly applying it to the surface of the cement. The I_t and F_t setting times were determined by the endpoint of the initial and final setting times of the needle tip to the first penetration measurement that did not mark the cement surface with a complete circular impression.[29]

2.4. Physicochemical Characterization. The composition phase of all of the cement samples after setting was studied by an X-ray diffractometer (XRD, GE, 3003TT, Germany) with a Cu Kα radiation source (λ = 1.54059 Å) operated at 40 kV. XRD patterns were recorded from 20 to 60° (2θ) with a 0.04 step size degree and a 2 s/step of counting time. The Fourier transform infrared (FTIR) spectra of the cement samples were registered in the spectrum from 400 to 4000 cm^{-1} with a wavelength resolution of 4 cm^{-1} using an IR

https://dx.doi.org/10.1021/acsomega.0c03927
ACS Omega 2021, 6, 2477−2486

spectrometer (FTIR, IRAffinity-1S, Shimadzu, Japan). The thermal degradation of the cement samples was examined using a thermogravimetric analyzer and a differential scanning calorimeter (STD-Q600 thermal analyzer, TA Instruments). The experiments were done at a heating rate of 20 K/min from 28 to 800 °C under a nitrogen atmosphere (100 mL/min).

2.5. Injectability Measurement and the Compressive Test. The powder mixture and the liquid mixture were blended manually for 1 min and then the paste was transferred into a 10 mL syringe with an inner diameter of 14.5 mm and a 16 G metal cannula with an outer diameter of 1.65 mm, an inner diameter of 1.19 mm, and a wall thickness of 0.22 mm. The filled syringes with cannulas were fixed perpendicular in a customized stand and positioned between the knock plates of a compression machine. This method was modified and adapted from Bohner et al.[12] The cement paste was introduced at a persistent velocity of 15 mm/min and as a function of the plunger displacement; the load was recorded. The test was terminated when the applied load extended a force of 120 N. The following equation is used to calculate the injectability percentage

$$\text{injectability}\ (\%) = \frac{W_F - W_A}{(W_F - W_E)} \times 100$$

where W_E is the weight of the vacant syringe, W_F is the weight of the syringe full of paste, and W_A is the weight of the syringe after the injection with any remaining paste in it.

The compressive test of the cement was performed using a Universal Testing Machine (Instron, 8801, MA) equipped with a 100 kN load cell on cylindrical cement samples (6 mm × 12 mm) at a strain rate of 0.5 mm/min in the dry state at room temperature. Each cement specimen was tested in triplicate. The ultimate compressive strength of the injectable cement samples was calculated from the stress−strain graph.

2.6. Morphology Observation. The cross section of the cement morphology was observed using a scanning electron microscope (SEM, Carl Zeiss, EVO 18, Germany) set off at 15 kV with a 10 mm working interspace. The samples were sputter-laminated with gold/palladium under high-rising vacuum at 20 kV (Quorum, SC7620) for 10 min.

2.7. *In Vitro* Tests. *2.7.1. Cell Culture and Toxicity Endpoint Evaluation.* Test samples (CHAXX, CsHAXX, CHAMg, CsHAMg, CHASr, and CSHAsr) were first sterilized by washing with 70% ethanol and later dried in a sterile chamber under low doses (207−222 nm) of far-UVC light. Mouse gingival fibroblast cells (GE1) were purchased from the RIKEN Cell Bank (RIKEN Cell Bank, Ibaraki, Japan) and cultured in an α culture medium, supplemented with 1% fetal bovine serum (FBS) (Biowest Inc., Riverside, MO) and antibiotic cocktail. The third passage cells were used at standard cell culture conditions (5% CO_2, 37 °C) with 1% (v/v) penicillin−streptomycin−neomycin (Sigma-Aldrich, St. Louis, MO) antibiotic cocktail in a cell culture chamber with standard parameters. Different concentration w/v ratios of injectable cement samples (0, 10, 25, 50, and 100 μg/mL) were mixed with the cell culture medium and incubated with cells for a 16 h period and under serum-free conditions. The 3-(4,5-dimethylthiazol-2-yl)-2,5-diphenyltetrazolium bromide (MTT) assay was employed to study the degree of toxicity to cells. The formazan crystals formed were lysed with 100 μL of the dimethyl sulfoxide (DMSO) solution. The resulting purple-colored product formed within the cells was spectrophotometrically measured at 570 nm (Multiskan FC, Thermo Fisher Scientific, Inc., PA), and the percentage of viable cells was calculated against control.

2.7.2. Time Dependency Test. To assess cell proliferation and its viability on the treatment with different injectable cements, the fibroblast cells (density of 1×10^4 cells/well) were seeded using 96-well plates. A standard dose as calculated from the toxicity endpoint study was used: 25 μg/mL CHAXX and CsHAXX, 50 μg/mL CHAMg and CsHAMg, and 10 μg/mL CHASr and CsHASr were incubated with different time intervals of 0, 6, 12, 18, and 24 h. After the treatments, the MTT solution was added to the cells followed by an incubation period of 3 h at 37 °C at cell culture concentrations. For the dissolution of the formazan crystals formed, cell lysis was done with 100 μL of the DMSO solution. The resulting purple-colored product formed within the cells was spectrophotometrically measured at 570 nm (Multiskan FC, Thermo Fisher Scientific, Inc., PA) and the percentage of viable cells was calculated against the control.

2.7.3. Cell Adhesion Study. The cell volume density evaluation (CVDE) assay was implemented in the gingival cells after the treatment with LD50 values of different injectable cement materials. Cells after stimulation to various time periods (as mentioned in Section 2.7.2) were washed with phosphate-buffered saline (PBS) using a crystal violet dye, which stained the DNA and gave a measure of the cell density. The excess dye was washed and removed, and the OD measured spectrophotometrically at 540 nm was directly proportional to the number of adherent cells in each well and was expressed as a percentage of the blank group.

2.7.4. Fluorometric Determination of Intracellular Reactive Oxygen Species (ROS). Intracellularly generated ROS was estimated and enumerated using an OxiSelect Intracellular ROS assay kit (DoJindo, Inc., Washington, DC). Cells seeded in 96-well culture vessels at a density of 1×10^3 cells/mL were incubated for 8 h with nonlethal concentrations of different injectables (the concentration was selected based on the MTT assay). Subsequently, Hank's balanced salt solution was used to wash the cells followed by 10 μM dichlorofluorescein diacetate (DCFH-DA) at 37 °C with an incubation period of 1 h in the dark. The amount of ROS-generated cells was measured by a fluorimeter at the activity and emission wavelengths of 485 and 530 nm.

2.7.5. Statistical Analysis. The experimental raw data for injectability between CHA (CHAXX, CHAMg, and CHASr) and CsHA (CsHAXX, CsHAMg, and CsHASr) cement paste samples were reported as mean ± standard deviation (SD) and Tukey's posttest for attaining statistical significance and analyzed by one-way analysis of variance (ANOVA). To find statistical significance, $p < 0.05$ was considered statistically significant using GraphPad Prism software v6.01. The data for *in vitro* toxicity is represented as the mean ± SD of three unpooled independent experiments. Two-tailed Student's *t*-test and Mann−Whitney *U*-test were used for comparisons within each parameter, while ANOVA and Dunnett *t*-tests were used for multiple comparisons; each of the number of treatment was compared with a single control. Differences were considered statistically significant when the *P*-value was <0.05.

3. RESULTS

3.1. Setting Time. The setting of the cement started rapidly after mixing the solid powder with an aqueous solution, whereas the setting reactions initiated evenly as the complete volume of the sample. The initial and final setting times are

https://dx.doi.org/10.1021/acsomega.0c03927
ACS Omega 2021, 6, 2477−2486

Table 1. Setting Time (Initial Time, I_t and Final Time, F_t) as Measured by the Gillmore Needle, the Percentage of the Remaining Weight After Heating at 800 °C from Thermogravimetric Analysis (TGA) Data, Injectable Force, and the Compressive Strength of the Prepared Calcium Phosphate Cement

sample	I_t (min)	F_t (min)	remaining weight (%)	injectability force (N)	compressive strength (MPa)
CHAXX	9.0 ± 0.5	13.1 ± 0.4	85.41	63.59 ± 8.91	1.78 ± 0.02
CHAMg	6.5 ± 0.3	11.0 ± 0.3	87.76	49.90 ± 2.90	1.57 ± 0.04
CHASr	7.2 ± 0.2	11.1 ± 0.0	89.31	40.72 ± 5.52	2.35 ± 0.03
CsHAXX	9.5 ± 0.3	13.4 ± 0.4	96.40	20.79 ± 1.11	1.76 ± 0.40
CsHAMg	8.0 ± 0.5	11.2 ± 0.1	94.85	32.33 ± 2.21	1.44 ± 0.13
CsHASr	8.5 ± 0.5	11.3 ± 0.8	93.51	36.39 ± 5.20	1.21 ± 0.00

summarized in Table 1. The initial and final setting times of CHA Mg^{2+}- and Sr^{2+}-doped cement (CHAMg and CHASr) were 7 and 11 min, which were faster than those of HA synthesized nondoped cement (CHAXX) (9 and 13 min, respectively). The initial and final setting times of Mg^{2+}- and Sr^{2+}-doped cement (CsHAMg and CsHASr) were 8 and 11 min, which were faster than those of CsHA nondoped cement (CsHAXX) (10 and 13 min, respectively). This showed that the setting time was lower in Mg^{2+}- and Sr^{2+}-doped cement than that of nondoped cement.

3.2. Physicochemical Properties. After complete setting and hardening for 24 h at room temperature, the final phase of all of the cement samples was examined by XRD (Figure 1).

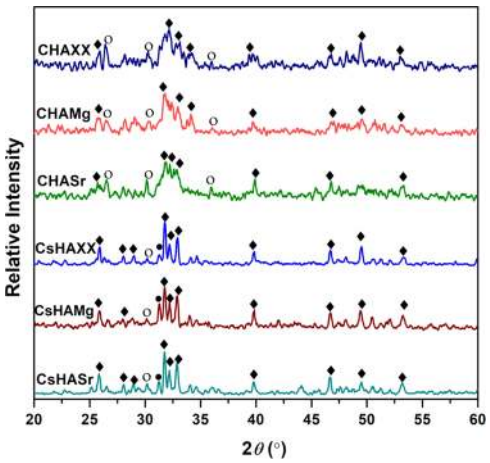

Figure 1. XRD patterns of calcium phosphate cement and peaks are indexed as (◆) hydroxyapatite, (○) anhydrous dicalcium phosphate, and (●) tricalcium phosphate.

All major peaks of the prepared cement were confirmed based on the ICDD powder diffraction database files (09-432: HA, 05-0586: DCPA, and 09-348: α-tricalcium phosphate (α-TCP)). The peak reflection at 25.9° and superposition of peaks at 31.8, 32.2, and 32.9° in CHA indicated the semicrystalline HA and CsHA cement indicated crystalline HA. The reflections at 26.4, 30.2, and 36.06° indicated unreacted residues of DCPA in CHAXX, CHAMg, and CHASr cements. In CsHA cement samples, the reflection at 26.4° indicated the unreacted residue of DCPA and the reflection at 30.8° indicated the presence of α-TCP. No other compounds or impurities of crystalline phases were identified besides these phases, and the end products between the cement samples after setting had no differences in phases.

The FTIR spectra (Figure 2) of the prepared cement powders identified the presence of the singular peaks of apatite. In Figure 2a, the spectral bands at 1025 and 960 cm^{-1} indicate

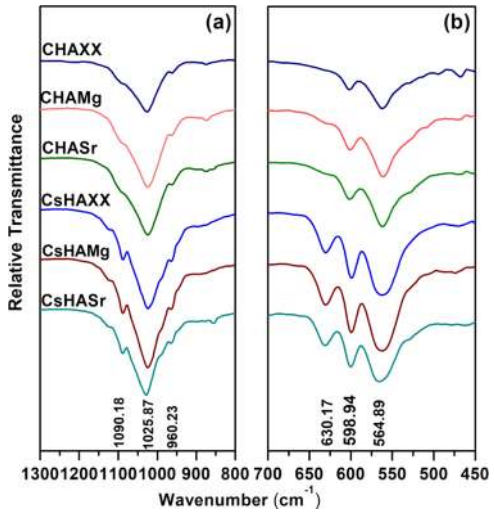

Figure 2. (a) FTIR spectra of the prepared calcium phosphate cements from (a) 1300 to 800 cm^{-1} and (b) from 700 to 450 cm^{-1}.

the presence of PO_4^{3-} components in HA cement samples (CHAXX, CHAMg, and CHASr). Meanwhile, in CsHA cement samples, the presence of PO_4^{3-} bonds was observed at 1090, 1025, and 960 cm^{-1} bonds of HA, as shown in Figure 2b. In CHA samples, the peaks at 598 and 564 cm^{-1} attributed to the PO_4^{3-} vibrational bands of HA indicated the weak crystalline degree of the cosubstituted apatitic phases with the weak resolution of all of the adsorption bands and also revealed a lack of the biological apatite hydroxyl peak. Meanwhile, in CsHA cement samples, the presence of PO_4^{3-} bonds was observed at 630, 598, and 564 cm^{-1} and indicated the bands of the pure form of HA. This indicates the existence of HA in both CHA- and CsHA-based cements.

The thermal degradation curves and their derivatives of cement samples are shown in Figure 3. The final weight losses of CHAMg and CHASr cements at 800 °C are 12.24 and 10.69%, respectively, whereas for CHAXX, it is 14.59%. The weight losses of CsHA and CsHASr at 800 °C are 5.15 and 6.49%, respectively, whereas for CsHAMg, it is 3.6%. Table 1 shows the remaining weight after heating at 800 °C. Figure 3b shows the first derivative curve of TGA and shows three distinctive processes for all of the cement samples. The weight loss that occurred between 196 and 300 °C in all samples was due to the evaporation of the residual water or moisture. The plateau between 380 and 460 °C can be due to the relocation of carbonate ions to the partial loss of CO_2 molecules.[30] The region between 590 and 670 °C appeared due to the decomposition of carbonate and phosphate molecules in the samples.

https://dx.doi.org/10.1021/acsomega.0c03927
ACS Omega 2021, 6, 2477−2486

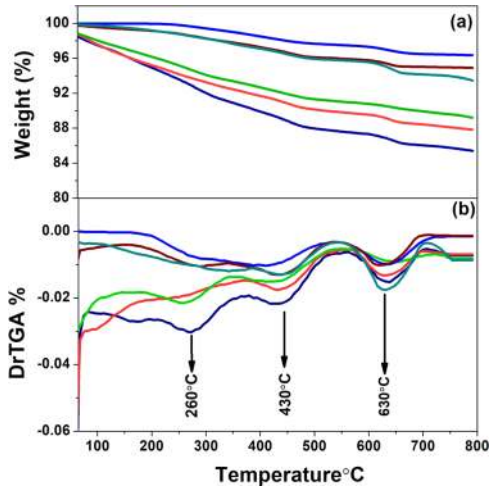

Figure 3. (a) TGA curves of the prepared calcium phosphate cement. (b) Derivative of TGA curves of the prepared calcium phosphate cements: CHAXX (dark navy blue line), CHAMg (red line), CHASr (light green line), CsHAXX (navy blue line), CsHAMg (brown line), and CsHASr (green line).

3.3. Injectability Measurement and the Compressive Test. The injectability behavior of the cement paste was studied under pressure and the load required for injectability was essential to understand the force required to inject the cement. Figure 4a,b displays the curves of extrusion (past extrusion force vs syringe plunger displacement) during injection of the paste and the percentage of cement extruded, respectively. Three distinct zones were observed in the injectability curve of the pastes. In the first zone, during the first few millimeters of displacement, the load was rapidly increased due to the applied load of the syringe plunger toward the cement. The force extrusion was defined by a slow plateau phase in the absence of phase separation and was slowly increased with low injectability in the second zone. In the third zone, the load increase represented the complete depletion until 120 N, where the load was stopped in the injection system.

The CHA-based cement without obvious filter pressing the cement was completely injected from the syringe. The graph curve shows an initial increase in the extrusion force, which constantly flattened to a plateau with small variations, which shows a steady injection of the cement paste. The injectability percentage of CHA cement samples (CHAXX, CHAMg, and CHASr) was recorded and was found to be above 90%. The CsHA-based cement was not fully injected from the syringe due to the filter pressing, which led to phase disengagement of the solid and liquid mixtures. The graph curve showed an initial acceleration in the extrusion force up to 20 N, and then phase separation was observed due to filter pressing, which led to clogging of the cement paste in the syringe. In the CsHA-based cement, the extrusion curve showed fluctuations in between the extrusion of the paste due to phase separation, which showed that the injectability of the cement paste was poor. The injectability percentage of the CsHAXX sample is 32.21%, while for the doped CsHA-based cements of CsHAMg and CsHASr, it is 27 and 30%, respectively. These results showed that the injectability percentage of CHA cement was higher than that of CsHA cement.

The compressive strength measured from the stress−strain curve is listed in Table 1. The compressive strength slightly

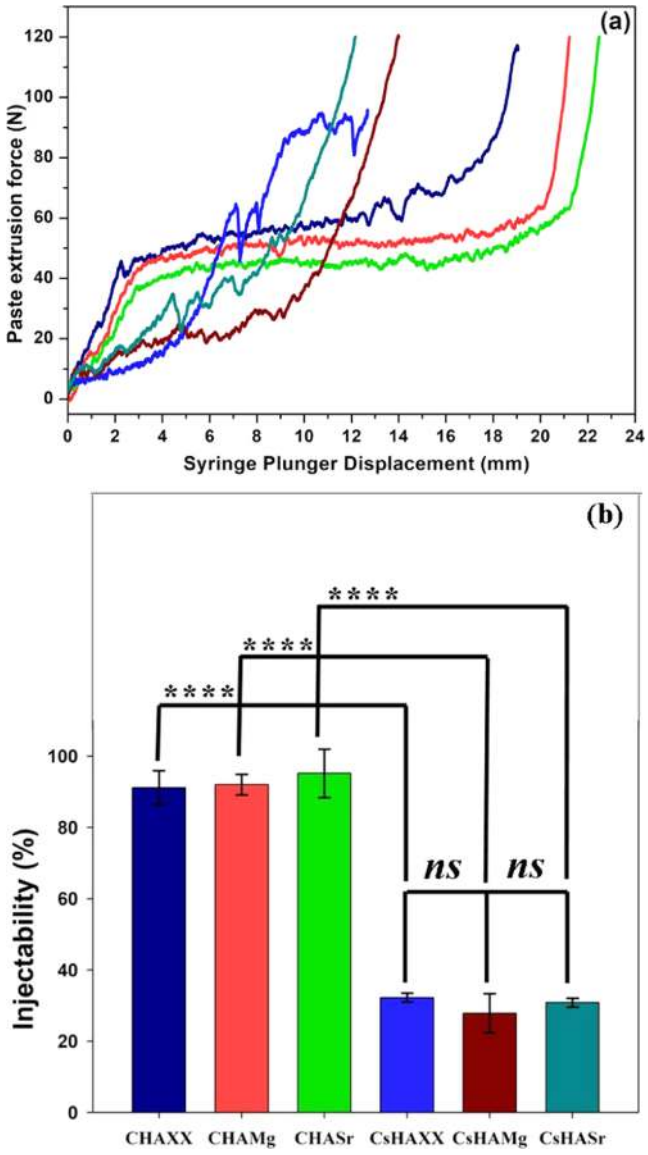

Figure 4. (a) Representative injection curves (load vs plunger displacement) of calcium phosphate cements: CHAXX (dark navy blue line), CHAMg (red line), CHASr (light green line), CsHAXX (navy blue line), CsHAMg (brown line), and CsHASr (green line). (b) Percentage of the injected calcium phosphate cement paste from the syringe, (where ****p < 0.0001 and ns = not significant (p > 0.05)).

reduced with the addition of Mg^{2+}-doped HA-based cement (CHAMg) and sintered HA-based cement (CsHAMg), when compared with undoped cements (CHAXX and CsHAXX). The Sr^{2+} ion-doped cement (CHASr) showed increased compressive strength, whereas decreased strength was observed in Sr^{2+} ion-doped sintered HA-based cement (CsHASr).

3.4. Microstructure Observation. The cross-sectional morphology of the different cement micrographs was investigated using SEM and is shown in Figure 5. The CHAXX cement consisted of bigger particles with a spherical shape, which agglomerated together to form clusters. The surfaces of CHAMg and CHASr cements were smooth except for some agglomerates and no cracks were observed. The surfaces of CsHAXX, CsHAMg, and CsHASr were rough with a dense arrangement of micron-size particles, which were

https://dx.doi.org/10.1021/acsomega.0c03927
ACS Omega 2021, 6, 2477−2486

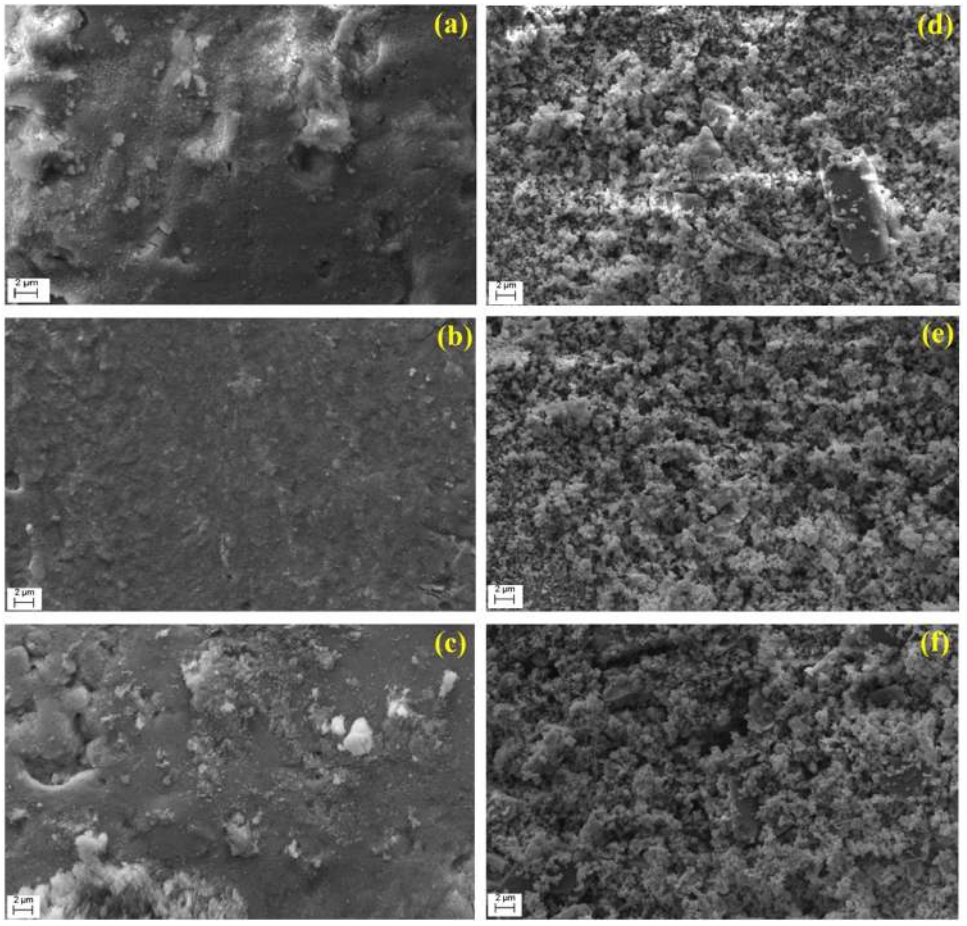

Figure 5. Scanning electron microscopy images of the cross-sectional view of cement samples (a) CHAXX, (b) CHAMg, and (c) CHASr showing smooth surfaces with some agglomerates. (d) CsHAXX, (e) CsHAMg, and (f) CsHASr showing a dense arrangement of microparticles on the surface at 6000× (scale bar is 2 μm).

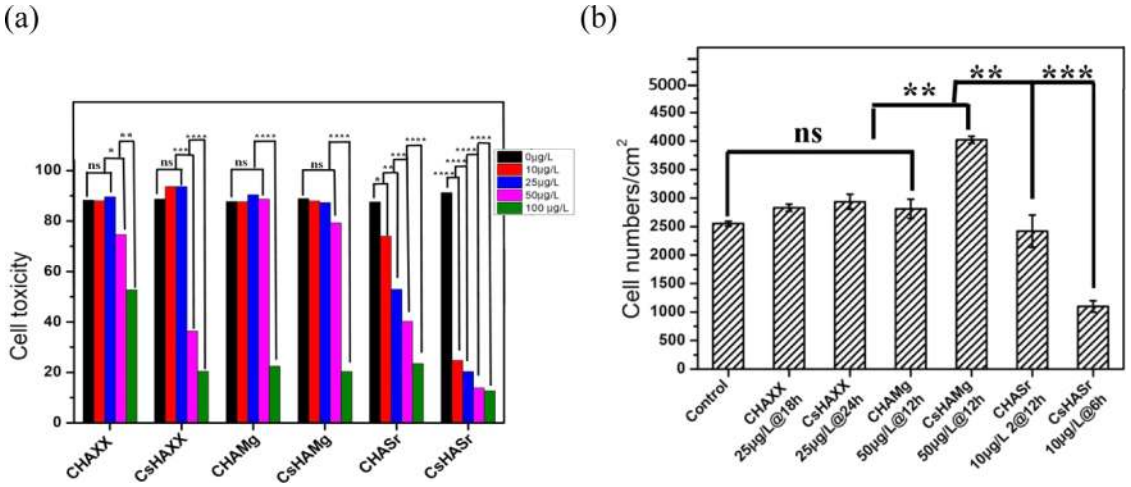

Figure 6. (a) Measurement of cell toxicity using mouse gingival fibroblast cells on cement samples was validated by the DNA fragmentation MTT assay. (b) Measurement of cell adhesion on cement samples using mouse gingival fibroblast cells, assessed at various concentrations at different time points. The cell adhesion level in Mg^{2+}-doped cement is higher in 12 h at 50 μg/L, whereas in Sr^{2+}-doped cement, cell adhesion is poor in 12 and 6 h at 10 μg/L. The cell adhesion in nondoped cement (CHAXX and CsHAXX) showed higher cell adhesion at different time points than the control sample (*p < 0.05, **p < 0.01, ***p < 0.001, ****p < 0.0001, and ns = not significant).

uniformly distributed. No pores were seen in the cement samples.

3.5. *In Vitro* Results. Evaluation of the toxicity endpoint of test materials was necessary to identify the suitability of materials for biomedical applications. The different cement samples displayed varying degrees of toxicity to cells in terms of concentrations, as shown in Figure 6a. Preliminary cell toxicity studies employing the MTT assay with different

https://dx.doi.org/10.1021/acsomega.0c03927
ACS Omega 2021, 6, 2477−2486

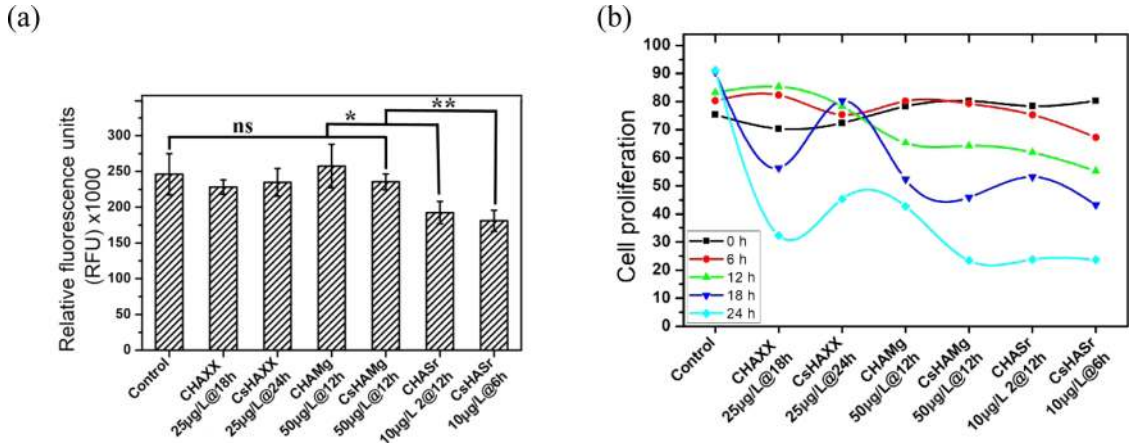

Figure 7. (a) Reactive oxygen species (ROS) produced by mouse gingival fibroblast cells treated with cement sample extracts for 8 h. Low ROS was produced in the cells treated with cement extracts compared to control. In contrast, Mg^{2+}-doped cement (CHAMg) was a potent inducer of the oxidative burst in GE1 compared with Sr^{2+}-doped cement samples. (b) Cell proliferation of mouse gingival fibroblast cells treated with different concentrations of cement sample extracts at different time points from 0 to 24 h. Mg^{2+}-doped cement (CHAMg) at 50 μg/L for 12 h shows good viability, whereas Sr^{2+}-doped cements (CHASr and CsHASr) at 10 μg/L for 12 and 6 h display lower cell viability at different time points (*p < 0.05, **p < 0.01, ***p < 0.001, ****p < 0.0001, and ns = not significant).

concentrations of cement showed that CHAXX, CsHAXX, CHAMg, and CsHAMg samples were nontoxic and did not affect the viability of fibroblast cells at 10, 25, and 50 μg/mL doses tested. Meanwhile, the CHASr and CsHASr samples showed significant cytotoxic effects and affected the viability of fibroblast cells at 25, 50, and, 100 μg/mL cement doses tested. Based on toxicity tests, the amount of cement is selected and the cell adhesion is estimated by mouse gingival fibroblast cells after the treatment with LD50 of different injectable cement materials. In Figure 6b, the viability of fibroblast adherent cells increased after 18 and 24 h on CHAXX and CsHAXX cement samples (25 μg/mL), which was observed spectrophotometrically at 540 nm. The cells attached to CHAMg and CsHAMg cement samples (50 μg/mL) were visible, in which CsHAMg samples showed significantly higher cell attachment in 12 h incubation. The cell attachment to CHASr and CsHASr cement samples (10 μg/mL) was significantly low, showing the poor adherence of fibroblast cells toward Sr^{2+}-doped cement samples.

Production of intracellular ROS is a hallmark of cell stress due to material toxicity. To understand the nonlethal concentration with suitable time incubation, we tested the ROS content by a spectrofluorometric assay for individual materials. The obtained results indicated that the Mg^{2+} and Sr^{2+} ion-based cement induced the generation of dose-dependent intracellular ROS. The results indicated that Sr^{2+}-doped cement samples (CHASr and CsHASr) induced significant cell stress (Figure 7a). Material toxicity and intracellular ROS production affected the cell population density. Therefore, we tested cell proliferation with different doses of materials at varying incubation times (dose and time of incubation were selected based on the MTT and time-dependent assays).

The cell proliferation at the initial 6 h of incubation with fibroblast cells shows that CHAXX, CHAMg, and CsHAMg cement samples have 80% proliferation, whereas CsHAXX, CHASr, and CsHASr cement samples have reduced to 75–70%. In 12 h of the incubation period, Sr^{2+}-doped cements (CHASr and CsHASr) show reduced cell proliferation of about 65 and 60%, respectively. In CsHAXX cement samples, the cell proliferation increased to 80% in 18 h of the incubation period, whereas the proliferation of CsHAXX, CHAMg, CsHAMg, CHASr, and CsHASr samples reduced to 50–60%. After 24 h of incubation of CsHAXX and CHAMg cement samples, the cell proliferation increased, whereas Sr^{2+}-doped cements (CHASr and CsHASr) and CsHAMg reduced the cell proliferation to 25% (Figure 7b). The *in vitro* toxicity and cell proliferation studies show that control CHAXX, CsHAXX, and CHAMg samples show reduced toxicity and increased cell proliferation toward fibroblast cells at different doses of materials at varied incubation times.

4. DISCUSSION

This study analyzed the properties of phosphate and carboxymethyl cellulose-based injectable calcium phosphate cement in which Mg^{2+} and Sr^{2+} ions were added and the final cement product was injected. The reaction mechanism for the injectable cement solidification followed the reaction kinetics for acid–base cement. Ions like Ca^{2+}, Sr^{2+}, Mg^{2+}, Si^{4+}, etc. would disintegrate in the cellulose- and phosphate-abundant acid solution upon blending of the components, dominating the generation of a natural solution network between the cations and the anions. This process will lead to gelation, saturation, and eventually precipitation to cause hardening of the cement by the connecting network.[31]

The ability of the cement to inject into the defect site and self-setting at body temperature is the major advantage of CPCs.[32] Therefore, it is preferable to develop rapid-setting cement that provides relatively high initial mechanical strength shortly after being placed in a defect site. Setting time is one of the prime factors in clinical applications, where long setting times may disintegrate cement pastes when they come into contact with physiological fluids or when bleeding occurs due to the failure to achieve complete hemostasis.[29] The Mg^{+2}- and Sr^{2+}-based cements are acceptable for clinical applications.[33,34] In this study, the Mg^{2+}- and Sr^{2+}-based cements with CMC achieved the ultimate setting time, which is very near to the initial setting time. This could be due to the gradual dissolution of Mg^{2+} and Sr^{2+} ions in the acidic solution and the released cations react with the phosphate anions to give acid–base reactions. This response of acid–base forms a

https://dx.doi.org/10.1021/acsomega.0c03927
ACS Omega 2021, 6, 2477–2486

network that hardens the cement faster.[35] The setting activity is very rapid and the conversion from paste to the solid phase takes about 3−4 min once the early setting time has been attained. The initial setting time prevailed when solid phases were mixed with phosphate aqueous salt liquid. The aqueous solution along with the solid phase can take part in the acceleration of dissolution, diffusion, reaction rate, and crystallization of the cement.[36,37]

The XRD phase shows the pattern of hydroxyapatite in the presence of anhydrous dicalcium phosphate with the addition of CMC and phosphate salt as the liquid part. The XRD phases of CHAXX, CHAMg, and CHASr cement samples appear to be semicrystalline in nature and the CsHAXX, CsHAMg, and CsHASr cement samples have a highly crystalline structure nature like enamel and dentine. The presence of tricalcium phosphate (TCP) at 31.2° in CsHA cement samples maybe due to the sintering of HA at a high temperature or incomplete decomposition of HA to TCP. The FTIR spectrum of the prepared cement confirms the existence of the distinctive apatite. In Figure 2a, the small crystalline degree of the cosubstituted apatite phases in CHA samples shows the feeble resolution of all the adsorption bands. They showed triply degenerated asymmetric stretching of the apatitic PO_4^{3-} groups, mainly a broadband at about 1025 cm^{-1} and shoulders at about 1090 and 960 cm^{-1}. The slight shifting of this band occurred because of incorporation of foreign ions into the lattice.[38,39] In Figure 2b, the spectra did not show the band at 630 cm^{-1} in CHA cement samples, which were attributable to the vibrational modes of the apatitic OH groups, indicating a lack of biological apatites in the hydroxyl group.[40] This detection was due to the microwave synthesis of HA as well as due to the achievable replacement of the OH groups by CO_3^{2-}. Meanwhile, the peak at 630 cm^{-1} in CsHA cement samples indicated the presence of the OH group as a characteristic of crystalline hydroxyapatite cement.

A relatively pronounced weight loss of all cement samples occurs in three stages of thermal analysis. The weight loss observed between 28 and 300 °C is the associated endothermic peak, which is attributed to the absorbed water. The decomposition of carbonate into CO_2 gas occurs from 350 and 450 °C. The dominating weight loss that occurs between 600 and 680 °C corresponds to the evaporation, desorption, and burning of CO_3^{2-} and HPO_4^{-}.[30] The SEM morphology for CsHAXX, CsHAMg, and CsHASr samples showed a more homogeneous structure. These results are possibly due to the development of the acid−base reaction on the surface energy of powders, which in turn enhance the convenient sites for nucleation.[37]

In CHA samples (Figure 4a), the load necessary for the paste to be injected gradually increased and phase separation took place owing to the continuous reduction in the L/P ratio of the paste inside the syringe.[41,42] However, there was a sudden expansion in the load, when obstruction of the syringe and needle occurred either impermanently or irrepairably, due to the impermeability of the clutter setup, which intercepted further injection.[43] In CsHA cement samples, phase segregation or obstruction of the syringe and needle was measured and observed by the load *versus* plunger displacement run curves and was characteristic of dissimilar occurrence during paste extrusion. The impenetrable aggregates block the syringe totally, stop the passing of the paste due to obstruction, and result in an abrupt and temporary rise in the load. However, it is true that the injectability percentages of sintered HA cement samples (CsHAXX, CsHAMg, and CsHASr) are low and the phase separation occur between the powder and the liquid, where the CHA samples show smooth injection of paste from the syringe with the needle.

The characteristics of apatite cement have important effects on the strength of orthopedic, dental cement, and maxillofacial applications. The strength of samples can only be assigned to the existence of Mg^{2+} in the cement matrix. This lowers the mechanical cohesion of the bulk cement and could additionally act as an initiator of crack.[44,45] The compressive strength of Mg^{2+}-doped cement is similar to those of CHA and CsHA, which is mostly used for synthetic bone regeneration administration. Hydroxyapatite is formed between dissolution and precipitation of one or more calcium phosphates when mixed with water or phosphate salts in the prepared cements.[37] The apatitic cement is more resistant than brushite.[46] The untimely strength elevation by the Mg^{2+}-doped formulation has an edge over several clinical administrations, where the cement can be put through to average loading circumstance. $SrCO_3$-modified cement (CHASr), on the other hand, increased the compressive strength by 2.35 MPa, whereas CsHASr-modified cement decreased the compressive strength by 1.21 MPa, which means that the crystalline nature of the cement would reduce the strength of the cement.

Despite the clinical advantages of calcium phosphate cement, only a few reports are available regarding the biocompatibility and cytotoxicity of these cement materials. The relation between cytotoxicity and the products derived from the setting reaction is still unknown. Cytotoxicity data were related to the remineralizing kinetics of the released calcium, phosphate, and different ions present in the composite cement. The studies have shown that Mg^{2+} and Sr^{2+} ions can stimulate cytotoxic outcomes of cells both *in vivo* and *in vitro*.[47,48] It has been reported that the cytotoxic outcomes are dose-dependent and higher doses can stimulate apoptosis.[25,49] In this study, different concentrations of cement samples displayed varying degrees of toxicity to cells, and 2 wt % Sr^{2+}-doped cement samples (CHASr and CsHASr) induced significant cell stress.

5. CONCLUSIONS

In the present study, we reveal the addition of Mg^{2+} and Sr^{2+} ions in self-setting injectable CPC with improved material properties. The findings showed that the injectability of the synthesized HA-based cement (CHA) paste was smooth and delivered completely following injection. The final product after setting was identified to be different phases of HA. Also, in toxicity study, the effect of magnesium(II)- and strontium-(II)-based calcium phosphate cements on mouse gingival fibroblast cells (GE1) has been studied. The 2 wt % Mg^{2+} and Sr^{2+} ion-doped cement sustainably released between 10 and 100 μg/mL, under *in vitro* conditions, whereas strontium ion concentrations show a significant degree of toxicity at 12 and 6 h incubation times. In ROS studies, cell adherence was observed in Mg^{2+}-doped cements, whereas the CsHASr sample expressed cell detachment after treatment. The reported data suggest that Mg^{2+}-doped self-setting cement opens an interesting way to easy filling of minimal invasive bone substitution and bone defects. The prepared injectable cement is purely synthetic and less expensive, which is an added advantage.

https://dx.doi.org/10.1021/acsomega.0c03927
ACS Omega 2021, 6, 2477−2486

AUTHOR INFORMATION

Corresponding Author

Inderchand Manjubala − *Department of Biosciences, School of Bio Sciences and Technology, Vellore Institute of Technology, Vellore 632014, India;* orcid.org/0000-0003-4873-2377; Email: i.manjubala@vit.ac.in

Authors

Vetharaj HephzibahRajam Arkin − *Department of Biosciences, School of Bio Sciences and Technology, Vellore Institute of Technology, Vellore 632014, India*

Uttamchand Narendrakumar − *Department of Manufacturing Engineering, School of Mechanical Engineering, Vellore Institute of Technology, Vellore 632014, India*

Harishkumar Madhyastha − *Department of Applied Physiology, Faculty of Medicine, University of Miyazaki, Miyazaki 8891692, Japan;* orcid.org/0000-0002-7143-4821

Complete contact information is available at: https://pubs.acs.org/10.1021/acsomega.0c03927

Author Contributions

I.M. formulated the concept, idea, and methodology, discussed, and contributed for framing and writing the review manuscript. V.H.A. contributed to the manuscript writing, and H.M. performed the *in vitro* experiment and analysis and also contributed to the manuscript writing. U.N. and I.M. did the idea implementation and manuscript reviewing and finalized the manuscript. The manuscript was written through contributions of all authors. All authors have given approval to the final version of the manuscript.

Notes

The authors declare no competing financial interest.

ACKNOWLEDGMENTS

This work was partially funded by VIT SEED Grant and SBST Faculty Research fund. V.H.A. acknowledges the fellowship support from VIT Research Associateship and scholar research grant every year from SBST. The authors also thank School of Advanced Sciences for TGA Characterization and School of Biosciences and Technology for DST-FIST cum VIT funded SEM facility and Advance Material Processing and Testing Lab, School of Mechanical Engineering for providing mechanical testing facility.

REFERENCES

(1) Stanovici, J.; Le Nail, L.-R.; Brennan, M.; Vidal, L.; Trichet, V.; Rosset, P.; Layrolle, P. Bone regeneration strategies with bone marrow stromal cells in orthopaedic surgery. *Cur. Res. Transl. Med.* **2016**, *64*, 83−90.

(2) Wang, P.; Zhao, L.; Liu, J.; Weir, M. D.; Zhou, X.; Xu, H. H. Bone tissue engineering via nanostructured calcium phosphate biomaterials and stem cells. *Bone Res.* **2014**, *2*, No. 14017.

(3) Manjubala, I.; Liu, Y.; Epari, D. R.; Roschger, P.; Schell, H.; Fratzl, P.; Duda, G. Spatial and temporal variations of mechanical properties and mineral content of the external callus during bone healing. *Bone* **2009**, *45*, 185−192.

(4) Manjubala, I.; Woesz, A.; Pilz, C.; Rumpler, M.; Fratzl-Zelman, N.; Roschger, P.; Stampfl, J.; Fratzl, P. Biomimetic mineral-organic composite scaffolds with controlled internal architecture. *J. Mater. Sci.: Mater. Med.* **2005**, *16*, 1111−1119.

(5) Habraken, W.; Habibovic, P.; Epple, M.; Bohner, M. Calcium phosphates in biomedical applications: materials for the future? *Mater. Today* **2016**, *19*, 69−87.

(6) Delgado-Ruiz, R. A.; Calvo Guirado, J. L.; Romanos, G. E. Bone grafting materials in critical defects in rabbit calvariae. A systematic review and quality evaluation using ARRIVE guidelines. *Clin. Oral Implants Res.* **2018**, *29*, 620−634.

(7) Zhang, Q.; Wu, W.; Qian, C.; Xiao, W.; Zhu, H.; Guo, J.; Meng, Z.; Zhu, J.; Ge, Z.; Cui, W. Advanced biomaterials for repairing and reconstruction of mandibular defects. *Mater. Sci. Eng., C* **2019**, *103*, No. 109858.

(8) O'Neill, R.; McCarthy, H.; Montufar, E.; Ginebra, M.-P.; Wilson, D.; Lennon, A.; Dunne, N. Critical review: Injectability of calcium phosphate pastes and cements. *Acta Biomater.* **2017**, *50*, 1−19.

(9) de Lacerda Schickert, S.; Jansen, J. A.; Bronkhorst, E. M.; van den Beucken, J. J.; Leeuwenburgh, S. C. Stabilizing dental implants with a fiber-reinforced calcium phosphate cement: an in vitro and in vivo study. *Acta Biomater.* **2020**, 280.

(10) Yousefi, A.-M. A review of calcium phosphate cements and acrylic bone cements as injectable materials for bone repair and implant fixation. *J. Appl. Biomater. Funct. Mater.* **2019**, *17*, No. 2280800019872594.

(11) Lopez-Heredia, M. A.; Kamphuis, G. B.; Thüne, P. C.; Öner, F. C.; Jansen, J. A.; Walboomers, X. F. An injectable calcium phosphate cement for the local delivery of paclitaxel to bone. *Biomaterials* **2011**, *32*, 5411−5416.

(12) Bohner, M.; Baroud, G. Injectability of calcium phosphate pastes. *Biomaterials* **2005**, *26*, 1553−1563.

(13) Liu, W.; Zhang, J.; Rethore, G.; Khairoun, K.; Pilet, P.; Tancret, F.; Bouler, J.-M.; Weiss, P. A novel injectable, cohesive and toughened Si-HPMC (silanized-hydroxypropyl methylcellulose) composite calcium phosphate cement for bone substitution. *Acta Biomater.* **2014**, *10*, 3335−3345.

(14) Liu, W.; Zhang, J.; Weiss, P.; Tancret, F.; Bouler, J.-M. The influence of different cellulose ethers on both the handling and mechanical properties of calcium phosphate cements for bone substitution. *Acta Biomater.* **2013**, *9*, 5740−5750.

(15) Manjubala, I.; Basu, P.; Narendrakumar, U. In situ synthesis of hydroxyapatite/carboxymethyl cellulose composites for bone regeneration applications. *Colloid Polym. Sci.* **2018**, *296*, 1729−1737.

(16) Bohner, M. Design of ceramic-based cements and putties for bone graft substitution. *Eur. Cell Mater.* **2010**, *20*, 1−12.

(17) Nabiyouni, M.; Brückner, T.; Zhou, H.; Gbureck, U.; Bhaduri, S. B. Magnesium-based bioceramics in orthopedic applications. *Acta Biomater.* **2018**, *66*, 23−43.

(18) Ostrowski, N.; Roy, A.; Kumta, P. N. Magnesium phosphate cement systems for hard tissue applications: a review. *ACS Biomater. Sci. Eng.* **2016**, *2*, 1067−1083.

(19) Kanter, B.; Vikman, A.; Brückner, T.; Schamel, M.; Gbureck, U.; Ignatius, A. Bone regeneration capacity of magnesium phosphate cements in a large animal model. *Acta Biomater.* **2018**, *69*, 352−361.

(20) Wu, F.; Wei, J.; Guo, H.; Chen, F.; Hong, H.; Liu, C. Self-setting bioactive calcium−magnesium phosphate cement with high strength and degradability for bone regeneration. *Acta Biomater.* **2008**, *4*, 1873−1884.

(21) Zhang, J.; Ma, X.; Lin, D.; Shi, H.; Yuan, Y.; Tang, W.; Zhou, H.; Guo, H.; Qian, J.; Liu, C. Magnesium modification of a calcium phosphate cement alters bone marrow stromal cell behavior via an integrin-mediated mechanism. *Biomaterials* **2015**, *53*, 251−264.

(22) Wu, L.; Luthringer, B. J.; Feyerabend, F.; Schilling, A. F.; Willumeit, R. Effects of extracellular magnesium on the differentiation and function of human osteoclasts. *Acta Biomater.* **2014**, *10*, 2843−2854.

(23) Yang, F.; Yang, D.; Tu, J.; Zheng, Q.; Cai, L.; Wang, L. Strontium enhances osteogenic differentiation of mesenchymal stem cells and in vivo bone formation by activating Wnt/catenin signaling. *Stem Cells* **2011**, *29*, 981−991.

(24) Guo, D.; Xu, K.; Zhao, X.; Han, Y. Development of a strontium-containing hydroxyapatite bone cement. *Biomaterials* **2005**, *26*, 4073−4083.
(25) Cohen-Solal, M. Strontium overload and toxicity: impact on renal osteodystrophy. *Nephrol., Dial., Transplant.* **2002**, *17*, 30−34.
(26) Schrooten, I.; Behets, G. J.; Cabrera, W. E.; Vercauteren, S. R.; Lamberts, L. V.; Verberckmoes, S. C.; Bervoets, A. J.; Dams, G.; Goodman, W. G.; De Broe, M. E.; D'Haese, P. C. Dose-dependent effects of strontium on bone of chronic renal failure rats. *Kidney Int.* **2003**, *63*, 927−935.
(27) Manjubala, I.; Sivakumar, M. In-situ synthesis of biphasic calcium phosphate ceramics using microwave irradiation. *Mater. Chem. Phys.* **2001**, *71*, 272−278.
(28) Takagi, S.; Chow, L. C. Formation of macropores in calcium phosphate cement implants. *J. Mater. Sci.: Mater. Med.* **2001**, *12*, 135−139.
(29) Kim, S. Y.; Jeon, S. H. Setting properties, mechanical strength and in vivo evaluation of calcium phosphate-based bone cements. *J. Ind. Eng. Chem.* **2012**, *18*, 128−136.
(30) Ivanova, T.; Frank-Kamenetskaya, O.; Kol'tsov, A.; Ugolkov, V. Crystal structure of calcium-deficient carbonated hydroxyapatite. Thermal decomposition. *J. Solid State Chem.* **2001**, *160*, 340−349.
(31) Boanini, E.; Gazzano, M.; Bigi, A. Ionic substitutions in calcium phosphates synthesized at low temperature. *Acta Biomater.* **2010**, *6*, 1882−1894.
(32) Ghosh, S.; Wu, V.; Pernal, S.; Uskoković, V. Self-setting calcium phosphate cements with tunable antibiotic release rates for advanced antimicrobial applications. *ACS Appl. Mater. Interfaces* **2016**, *8*, 7691−7708.
(33) Golafshan, N.; Vorndran, E.; Zaharievski, S.; Brommer, H.; Kadumudi, F. B.; Dolatshahi-Pirouz, A.; Gbureck, U.; van Weeren, R.; Castilho, M.; Malda, J. Tough magnesium phosphate-based 3D-printed implants induce bone regeneration in an equine defect model. *Biomaterials* **2020**, *261*, No. 120302.
(34) Schumacher, M.; Gelinsky, M. Strontium modified calcium phosphate cements−approaches towards targeted stimulation of bone turnover. *J. Mater. Chem. B* **2015**, *3*, 4626−4640.
(35) Zhou, H.; Agarwal, A. K.; Goel, V. K.; Bhaduri, S. B. Microwave assisted preparation of magnesium phosphate cement (MPC) for orthopedic applications: a novel solution to the exothermicity problem. *Mater. Sci. Eng., C* **2013**, *33*, 4288−4294.
(36) Riman, R. E.; Suchanek, W. L.; Lencka, M. M. Hydrothermal crystallization of ceramics. *Ann. Chim. Sci. Mater.* **2002**, 15−36.
(37) Zhang, J.; Liu, W.; Schnitzler, V.; Tancret, F.; Bouler, J.-M. Calcium phosphate cements for bone substitution: chemistry, handling and mechanical properties. *Acta Biomater.* **2014**, *10*, 1035−1049.
(38) Youness, R. A.; Taha, M. A.; Elhaes, H.; Ibrahim, M. Molecular modeling, FTIR spectral characterization and mechanical properties of carbonated-hydroxyapatite prepared by mechanochemical synthesis. *Mater. Chem. Phys.* **2017**, *190*, 209−218.
(39) Liou, S.-C.; Chen, S.-Y.; Lee, H.-Y.; Bow, J.-S. Structural characterization of nano-sized calcium deficient apatite powders. *Biomaterials* **2004**, *25*, 189−196.
(40) Rey, C.; Combes, C.; Drouet, C.; Sfihi, H.; Barroug, A. Physico-chemical properties of nanocrystalline apatites: Implications for biominerals and biomaterials. *Mater. Sci. Eng., C* **2007**, *27*, 198−205.
(41) Habib, M.; Baroud, G.; Gitzhofer, F.; Bohner, M. Mechanisms underlying the limited injectability of hydraulic calcium phosphate paste. *Acta Biomater.* **2008**, *4*, 1465−1471.
(42) Habib, M.; Baroud, G.; Gitzhofer, F.; Bohner, M. Mechanisms underlying the limited injectability of hydraulic calcium phosphate paste. Part II: Particle separation study. *Acta Biomater.* **2010**, *6*, 250−256.
(43) Mason, M. S.; Huang, T.; Landers, R. G.; Leu, M. C.; Hilmas, G. E. Aqueous-based extrusion of high solids loading ceramic pastes: Process modeling and control. *J. Mater. Process. Technol.* **2009**, *209*, 2946−2957.
(44) Geffers, M.; Groll, J.; Gbureck, U. Reinforcement strategies for load-bearing calcium phosphate biocements. *Materials* **2015**, *8*, 2700−2717.
(45) Jia, J.; Zhou, H.; Wei, J.; Jiang, X.; Hua, H.; Chen, F.; Wei, S.; Shin, J.-W.; Liu, C. Development of magnesium calcium phosphate biocement for bone regeneration. *J. R. Soc., Interface* **2010**, *7*, 1171−1180.
(46) Sarkar, S. K.; Lee, B. Y.; Padalhin, A. R.; Sarker, A.; Carpena, N.; Kim, B.; Paul, K.; Choi, H. J.; Bae, S.-H.; Lee, B. T. Brushite-based calcium phosphate cement with multichannel hydroxyapatite granule loading for improved bone regeneration. *J. Biomater. Appl.* **2016**, *30*, 823−837.
(47) Di Virgilio, A. L.; Reigosa, M.; de Mele, M. F. L. Biocompatibility of magnesium particles evaluated by in vitro cytotoxicity and genotoxicity assays. *J. Biomed. Mater. Res., Part B* **2011**, *99B*, 111−119.
(48) Er, K.; Polat, Z. A.; Özan, F.; Taşdemir, T.; Sezer, U.; Siso, Ş. H. Cytotoxicity analysis of strontium ranelate on cultured human periodontal ligament fibroblasts: a preliminary report. *J. Formosan Med. Assoc.* **2008**, *107*, 609−615.
(49) Wolf, F. I.; Trapani, V.; Cittadini, A. Magnesium and the control of cell proliferation: looking for a needle in a haystack. *Magnesium Res.* **2008**, *21*, 83−91.

https://dx.doi.org/10.1021/acsomega.0c03927
ACS Omega 2021, 6, 2477−2486